

# A Variational Constitutive Model for Porous Metal Plasticity

Kerstin Weinberg<sup>1</sup>, Alejandro Mota<sup>1</sup>, Michael Ortiz<sup>1</sup>

Division of Engineering and Applied Science, California Institute of Technology, Pasadena, CA 91125, USA

Received: April 5, 2005/ Revised version: April 5, 2005

**Abstract** This paper presents a variational formulation of viscoplastic constitutive updates for porous elasto-plastic materials. The material model combines von Mises plasticity with volumetric plastic expansion as induced, e.g., by the growth of voids and defects in metals. The finite deformation theory is based on the multiplicative decomposition of the deformation gradient and an internal variable formulation of continuum thermodynamics. By the use of logarithmic and exponential mappings the stress update algorithms are extended from small strains to finite deformations. Thus the time-discretized version of the porous-viscoplastic constitutive updates is described in a fully variational manner. The range of behavior predicted by the model and the performance of the variational update are demonstrated by its application to the forced expansion and fragmentation of U-6%Nb rings.

## 1 Introduction

Most metals and alloys contain a certain amount of arbitrarily distributed cavities, with their growth and finally coalescence being the basic failure mechanism in ductile fracture. Typically the size of the cavities (voids) is small compared to the size of the body, and their distribution is defined by a characteristic function  $\chi = \chi(x), x \in \mathbb{R}^3$ . The spatial average over the current volume of the body  $V$  defines the void volume fraction or porosity

$$f = \frac{1}{V} \int_V \chi(x) dx, \quad (1.1)$$

which is, for typical engineering materials, initially in the range of  $10^{-2}$  to  $10^{-4}$  [26; 23]. It is known from experiments that the voids start to coalesce and eventually ductile failure occurs when the porosity of the material reaches values from 0.1 to 0.3 [3; 21; 6]. Observations of the fracture surface show that it is typically dimpled. The aim of our work is to provide a variational framework to simulate this process using the finite element method.

The classical yield condition for porous ductile materials was developed by Gurson [10], who, like most subsequent authors, exploits the idea that the physical process of damage in ductile media may be described by the structural behavior of simple representative volume elements. Tvergaard and Needleman [28] introduced a bilinear function which accounts for an accelerated growth of voids due to the effect of coalescence after reaching an empirical critical void volume fraction. Termed the Gurson-Tvergaard-Needleman model, it became the conventional criterion for ductile fracture problems.

One relevant result in the understanding of void growth is the concept of critical cavitation pressure. When the hydrostatic tension is sufficiently high, the voids inside a material grow with no bounds even through the remote stresses and strains are kept constant. The existence of such an instability was recognized for nonlinear elastic solids by Ball [1] and later determined for quasistatic elasto-plastic solids by Huang et al. [12; 27].

At very high strain rates ( $\dot{\epsilon} > 10^6 s^{-1}$ ) the typical void growth turns out to be very different to the quasistatic case. In general, extremely high stress levels, especially very high hydrostatic tensions, are developed and inertial stresses are not longer negligible. Upon impact, compressive stress waves travel through the body which, by reflection and superposition, may induced high tension and the material will fail dynamically. This process, known as spallation, has been studied extensively (cf. [2; 5; 8; 30]). The spall strength of the material, which is determined by impact-spallation experiments, is related to the critical cavitation pressure under shock-load conditions.

Ortiz and Molinari [18] analyzed the dynamic expansion of a single spherical void in an infinite rigid plastic medium under the action of remote hydrostatic tension. They reported that if the initial void radius increases by at least one order of magnitude, the void growth is dominated by microinertial effects, whereas the effect of rate dependence of the material and the plastic dissipative effects play a secondary role. Under the regime of rapidly applied, supercritical hydrostatic tension the void radius grows unbounded as a linear func-

tion of time. Tong and Ravichandran [25] and Thomason [24] draw similar conclusions, and they also emphasize the strong stabilizing effect of microinertia on the void growth process which consequently delays coalescence of the voids. High accelerations sustained by the material particles in the vicinity of voids result in significant inertial effects, particularly for materials with low strain-rate sensitivity [17].

In this paper we present a variational constitutive model for porous plastic materials under static and dynamic loading conditions. The constitutive framework used here is based on a multiplicative decomposition of the deformation gradient into an elastic part and an inelastic part, and on a conventional internal-variable formulation of continuum thermodynamics, cf. [15; 20]. Using a relatively simple dilute model we link the mechanism of plastic expansion and global softening of the material to parameters which describe the micromechanical mechanisms of void growth; avoiding altogether the need of macroscopic failure criteria.

## 2 General framework

We start by providing a simple framework for integrating a conventional model of deviatoric plasticity, such as  $J_2$ -flow theory, to an equation of state representing the effective macroscopic behavior of a void ensemble.

### 2.1 Constitutive relations

The thermo-mechanical response of the solids considered here is characterized by a free-energy density per unit undeformed volume of the form

$$A = A(\mathbf{F}, \mathbf{F}^p, \epsilon^p, \theta^p, T), \quad (2.1)$$

where  $\mathbf{F}$  is the deformation gradient,  $\mathbf{F}^p$  is the plastic part of the deformation gradient,  $\epsilon^p \geq 0$  is an effective deviatoric plastic strain,  $\theta^p \geq 0$  is an effective volumetric plastic strain,  $T$  is the absolute temperature, and

$$\mathbf{F}^e = \mathbf{F} \mathbf{F}^{p-1} \quad (2.2)$$

is the elastic part of the deformation gradient [14].

The plastic deformation rate is assumed to obey the flow rule

$$\dot{\mathbf{F}}^p \mathbf{F}^{p-1} = \dot{\epsilon}^p \mathbf{M} + \dot{\theta}^p \mathbf{N}, \quad (2.3)$$

where  $\dot{\epsilon}^p$  and  $\dot{\theta}^p$  are subject to the irreversibility constraints

$$\dot{\epsilon}^p \geq 0, \quad \dot{\theta}^p \geq 0, \quad (2.4)$$

and the tensors  $\mathbf{M}$  and  $\mathbf{N}$  set the direction of the deviatoric and volumetric plastic deformation rates, respectively, and which are assumed to satisfy

$$\text{tr} \mathbf{M} = 0, \quad \mathbf{M} \cdot \mathbf{M} = \frac{3}{2}, \quad \mathbf{N} = \pm \frac{1}{3} \mathbf{I}, \quad (2.5)$$

with the plus sign in  $\mathbf{N}$  corresponding to void expansion, and the minus sign to void collapse. The tensors  $\mathbf{M}$  and  $\mathbf{N}$  are

otherwise unknown and are to be determined as part of the solution. The constraints (2.5) may be regarded as defining the assumed kinematics of plastic deformation. As we shall see, the direction of plastic deformation, as determined by  $\mathbf{M}$  and  $\mathbf{N}$ , follows from the variational structure of the constitutive update in a manner which generalizes the principle of maximum dissipation [11; 20].

For purely volumetric deformations the flow rule (2.3) reduces to

$$\frac{d}{dt} \log J^p = \text{tr} \mathbf{N} \dot{\theta}^p = \pm \dot{\theta}^p, \quad (2.6)$$

where the plus sign corresponds to void expansion and the minus sign to void collapse. From (2.6) we find

$$\dot{\theta}^p = \left| \frac{d}{dt} \log J^p \right|, \quad \theta^p(t) = \theta^p(0) + \int_0^t \dot{\theta}^p(\xi) d\xi, \quad (2.7)$$

i.e., the variable  $\theta^p$  is a measure of the *accumulated* volumetric plastic deformation. Evidently,  $\theta^p$  and  $\log J^p$  coincide up to a constant for monotonic expansion, but the distinction between the two variables becomes important for arbitrary loading combining alternating phases of void expansion and collapse.

The first Piola-Kirchhoff stress tensor  $\mathbf{P}$  follows from Coleman's relations as

$$\mathbf{P} = \frac{\partial A}{\partial \mathbf{F}}, \quad (2.8)$$

while the thermodynamic force  $Y$  conjugate to the internal variable  $\epsilon^p$  is

$$Y = \sigma - \sigma_c = \mathbf{T} \cdot \frac{\partial \mathbf{F}^p}{\partial \epsilon^p} - \frac{\partial A}{\partial \epsilon^p}, \quad (2.9)$$

where

$$\sigma = \boldsymbol{\Sigma} \cdot \mathbf{M}, \quad \sigma_c = \frac{\partial A}{\partial \epsilon^p}, \quad (2.10)$$

are the effective deviatoric stress and the deviatoric flow stress, respectively, and we write

$$\boldsymbol{\Sigma} = \mathbf{T} \mathbf{F}^{pT}, \quad (2.11)$$

in which  $\mathbf{T}$  is the thermodynamic force conjugate to  $\mathbf{F}^p$ , written as

$$\mathbf{T} = -\frac{\partial A}{\partial \mathbf{F}} \cdot \frac{\partial \mathbf{F}}{\partial \mathbf{F}^p} - \frac{\partial A}{\partial \mathbf{F}^p} = \mathbf{F}^{eT} \mathbf{P} - A_{, \mathbf{F}^p}. \quad (2.12)$$

Likewise, the thermodynamic force  $Z$  conjugate to the internal variable  $\theta^p$  takes the form

$$Z = p - p_c = \mathbf{T} \cdot \frac{\partial \mathbf{F}^p}{\partial \theta^p} - \frac{\partial A}{\partial \theta^p}, \quad (2.13)$$

where

$$p = \boldsymbol{\Sigma} \cdot \mathbf{N}, \quad p_c = \frac{\partial A}{\partial \theta^p}, \quad (2.14)$$

are the effective pressure and the flow pressure, respectively.

Appropriate rate equations for the internal variables  $\epsilon^p$  and  $\theta^p$  must be specified to formulate a complete set of constitutive relations. With a view to ensuring a variational structure, we postulate the existence of a dual kinetic potential  $\psi^*(\dot{\epsilon}^p, \dot{\theta}^p, \mathbf{F}^p, T)$  such that

$$Y = \frac{\partial \psi^*}{\partial \dot{\epsilon}^p}, \quad Z = \frac{\partial \psi^*}{\partial \dot{\theta}^p}. \quad (2.15)$$

## 2.2 Variational formulation of the dynamic problem

Consider a body occupying a region  $B \subset \mathbb{R}^3$  and undergoing a deformation described by a mapping  $\varphi : B \times [t_1, t_2] \rightarrow \mathbb{R}^3$ . Suppose that the boundary  $\partial B$  is the disjoint union of a displacement boundary  $\partial_1 B$  and a traction boundary  $\partial_2 B$ . Let  $\rho_0 : B \times [t_1, t_2] \rightarrow \mathbb{R}$  denote the referential mass density per unit undeformed volume,  $\mathbf{B} : B \times [t_1, t_2] \rightarrow \mathbb{R}^3$  the applied body-force field,  $\bar{\varphi} : \partial_1 B \times [t_1, t_2] \rightarrow \mathbb{R}^3$  the prescribed boundary displacements,  $\bar{\mathbf{T}} : \partial_2 B \times [t_1, t_2] \rightarrow \mathbb{R}^3$  the applied tractions. For definiteness, we assume that the kinetic energy of the body is of the form

$$K = \int_B \frac{1}{2} \rho_0 |\dot{\varphi}|^2 dV + \int_B L(\dot{\mathbf{F}}^p, \mathbf{F}^p) dV, \quad (2.16)$$

where the first term represents the macroscopic inertia and the second term the microinertia attendant to plastic deformation. The first variation of  $K$  is

$$\begin{aligned} \delta \int_{t_1}^{t_2} K dt &= - \int_{t_1}^{t_2} \int_B \rho_0 \dot{\varphi} \cdot \delta \varphi dV dt + \\ &\int_{t_1}^{t_2} \int_B \left( \frac{\partial L}{\partial \mathbf{F}^p} - \frac{d}{dt} \frac{\partial L}{\partial \dot{\mathbf{F}}^p} \right) \cdot \delta \mathbf{F}^p dV dt, \end{aligned} \quad (2.17)$$

for all admissible variations  $\delta \varphi$  and  $\delta \mathbf{F}^p$ . The term in parenthesis may be regarded as an additional stress acting on  $\mathbf{F}^p$ , arising from microinertia. In addition, for every  $t \in [t_1, t_2]$  we introduce the power functional

$$\begin{aligned} \Phi[\dot{\varphi}, \dot{\epsilon}^p, \dot{\theta}^p, \mathbf{M}, \mathbf{N}] &= \\ &\int_B \left[ \dot{A} + \psi^* - \left( \frac{\partial L}{\partial \mathbf{F}^p} - \frac{d}{dt} \frac{\partial L}{\partial \dot{\mathbf{F}}^p} \right) \cdot \dot{\mathbf{F}}^p \right] dV - \\ &\int_B \rho_0 (\mathbf{B} - \dot{\varphi}) \cdot \dot{\varphi} dV - \int_{\partial_2 B} \bar{\mathbf{T}} \cdot \dot{\varphi} dS. \end{aligned} \quad (2.18)$$

where  $\mathbf{F}^p$ ,  $\epsilon^p$ ,  $\theta^p$ ,  $\mathbf{M}$  and  $\mathbf{N}$  are now regarded as fields over  $B$ , and  $\dot{\mathbf{F}}^p$  is determined by  $\dot{\epsilon}^p$ ,  $\dot{\theta}^p$ ,  $\mathbf{M}$  and  $\mathbf{N}$  through the flow rule (2.3). Using identities (2.8), (2.9) and (2.13) and the flow rule (2.3), (2.18) may be rewritten as

$$\begin{aligned} \Phi[\dot{\varphi}, \dot{\epsilon}^p, \dot{\theta}^p, \mathbf{M}, \mathbf{N}] &= \\ &\int_B (\mathbf{P} \cdot \text{Grad} \dot{\varphi} - Y \dot{\epsilon}^p - Z \dot{\theta}^p + \psi^*) dV - \\ &\int_B \rho_0 (\mathbf{B} - \dot{\varphi}) \cdot \dot{\varphi} dV - \int_{\partial_2 B} \bar{\mathbf{T}} \cdot \dot{\varphi} dS, \end{aligned} \quad (2.19)$$

where  $\mathbf{F} = \text{Grad} \varphi$  has been introduced, and with

$$\boldsymbol{\Sigma} = \mathbf{T} \mathbf{F}^{pT} + \left( \frac{\partial L}{\partial \mathbf{F}^p} - \frac{d}{dt} \frac{\partial L}{\partial \dot{\mathbf{F}}^p} \right) \mathbf{F}^{pT} \quad (2.20)$$

in place of (2.11). For every  $t \in [t_1, t_2]$ , the rates  $\dot{\varphi}$ ,  $\dot{\epsilon}^p$ ,  $\dot{\theta}^p$ , and the directions of plastic flow  $\mathbf{M}$  and  $\mathbf{N}$ , follow jointly from the minimization problem

$$\Phi^{\text{eff}}[\dot{\varphi}] = \inf_{\dot{\epsilon}^p, \dot{\theta}^p, \mathbf{M}, \mathbf{N}} \Phi[\dot{\varphi}, \dot{\epsilon}^p, \dot{\theta}^p, \mathbf{M}, \mathbf{N}], \quad (2.21)$$

subject to the constraints (2.4), (2.5). Problem (2.21) additionally defines the reduced power functional  $\Phi^{\text{eff}}[\dot{\varphi}]$ . The

material velocity field  $\dot{\varphi}$  finally follows from the minimization problem

$$\inf_{\dot{\varphi}} \Phi^{\text{eff}}[\dot{\varphi}], \quad \dot{\varphi} = \bar{\varphi} \text{ on } \partial_2 B. \quad (2.22)$$

Since the extended functional  $\Phi[\dot{\varphi}, \dot{\epsilon}^p, \dot{\theta}^p, \mathbf{M}, \mathbf{N}]$  does not depend on spatial derivatives of the fields, the minimization (2.21) may be effected locally, with the result

$$\begin{aligned} \Phi^{\text{eff}}[\dot{\varphi}] &= \\ &\int_B [\phi(\text{Grad} \dot{\varphi}) - \rho_0 (\mathbf{B} - \dot{\varphi}) \cdot \dot{\varphi}] dV - \int_{\partial_2 B} \bar{\mathbf{T}} \cdot \dot{\varphi} dS, \end{aligned} \quad (2.23)$$

where

$$\phi(\dot{\mathbf{F}}) = \inf_{\dot{\epsilon}^p, \dot{\theta}^p, \mathbf{M}, \mathbf{N}} f(\dot{\mathbf{F}}, \dot{\epsilon}^p, \dot{\theta}^p, \mathbf{M}, \mathbf{N}), \quad (2.24)$$

subject to the constraints (2.4), (2.5), and

$$f(\dot{\mathbf{F}}, \dot{\epsilon}^p, \dot{\theta}^p, \mathbf{M}, \mathbf{N}) = \mathbf{P} \cdot \dot{\mathbf{F}} - Y \dot{\epsilon}^p - Z \dot{\theta}^p + \psi^*, \quad (2.25)$$

is a power density per unit undeformed volume. Evidently, by the construction of the power functional the kinetic relations (2.15) are Euler-Lagrange equations of the minimum problem (2.24). The additional Euler-Lagrange equations with respect to  $\mathbf{M}$  and  $\mathbf{N}$  are

$$\boldsymbol{\Sigma} - \lambda_1 \mathbf{I} - \lambda_2 \mathbf{M} = \mathbf{0}, \quad \text{tr}(\boldsymbol{\Sigma}) - \lambda_3 \text{tr}(\mathbf{N}) = 0, \quad (2.26)$$

where  $\lambda_1$ ,  $\lambda_2$  and  $\lambda_3$  are Lagrange multipliers arising from the constraints (2.5). Using these constraints, eqs. (2.26) can be solved for  $\mathbf{M}$  and  $\mathbf{N}$ , with the result

$$\mathbf{M} = \frac{3 \text{dev}(\boldsymbol{\Sigma})}{2\sigma}, \quad \mathbf{N} = \frac{1}{3} \text{sgn}(\text{tr}(\boldsymbol{\Sigma})) \mathbf{I}, \quad (2.27)$$

where

$$\sigma = \sqrt{(3/2) \text{dev}(\boldsymbol{\Sigma}) \cdot \text{dev}(\boldsymbol{\Sigma})} \quad (2.28)$$

is the Mises effective stress. Using (2.27) in (2.3) we obtain

$$\dot{\mathbf{F}}^p \mathbf{F}^{p-1} = \dot{\epsilon}^p \frac{3 \text{dev}(\boldsymbol{\Sigma})}{2\sigma} + \frac{1}{3} \dot{\theta}^p \text{sgn}(\text{tr}(\boldsymbol{\Sigma})) \mathbf{I}, \quad (2.29)$$

which is an extension of the Prandtl-Reuss flow rule into the compressible range.

The power density function  $\phi(\dot{\mathbf{F}})$  has the fundamental property [20]

$$\mathbf{P} = \frac{\partial \phi}{\partial \dot{\mathbf{F}}}(\dot{\mathbf{F}}), \quad (2.30)$$

and, consequently, the Euler-Lagrange equations corresponding to the minimization problem (2.22) are the equations of motion

$$\begin{aligned} \text{Div} \mathbf{P} + \rho_0 \mathbf{B} &= \rho_0 \dot{\varphi} \quad \text{in } B, \\ \mathbf{P} \cdot \bar{\mathbf{N}} &= \bar{\mathbf{T}} \quad \text{on } \partial_2 B, \end{aligned} \quad (2.31)$$

where in the latter expression  $\bar{\mathbf{N}}$  is the unit normal to  $\partial B$ .

### 3 A simple void-growth model

We illustrate the application of the preceding general framework to the case of porous plasticity by means of a simple void-growth model. We specifically focus on conditions such as arise in shocked metals, involving high pressures, strain rates and non-negligible microinertia.

#### 3.1 Kinematics of void growth

Consider a representative sample of material of undeformed volume  $V_0$  and deformed volume  $V = JV_0$ . The local volume fraction of voids (1.1) in the undeformed configuration is

$$f_0 = N \frac{4\pi a_0^3}{3}, \quad (3.1)$$

where  $N$  is void density, i.e., the number of spherical voids per unit undeformed volume of the body, and  $a_0$  is the initial mean void radius in the representative volume. In addition, the volume of undeformed matrix material is  $(1 - f_0)V_0$ . Let now  $a$  denote the mean void radius in the intermediate, or plastically deformed, configuration. Assuming a spherical shell model with a plastically-incompressible matrix, and neglecting the elastic volume change of the voids, we have

$$J^p = 1 - f_0 + N \frac{4\pi a^3}{3}, \quad f = \frac{f_0 + J^p - 1}{J^p}. \quad (3.2)$$

This relation places the void radius  $a$  and  $J^p$  in one-to-one correspondence. In all subsequent expressions, we conventionally take  $J^p$  to be the primary independent variable and regard  $a$ , and its functions, as functions of  $J^p$  through (3.2).

#### 3.2 Elastic strain-energy density

Assume that the free-energy density (2.1) has the additive structure

$$A(\mathbf{F}, \mathbf{F}^p, \epsilon^p, \theta^p, T) = W^e(\mathbf{F}^e, T) + W^p(\epsilon^p, \theta^p, T), \quad (3.3)$$

where  $W^e(\mathbf{F}^e, T)$  and  $W^p(\epsilon^p, \theta^p, T)$  are the elastic and stored energy densities per unit undeformed volume, respectively. Then  $\sigma_c$  and  $p_c$  reduce to

$$\begin{aligned} \sigma_c(\epsilon^p, \theta^p, T) &= \frac{\partial W^p}{\partial \epsilon^p}(\epsilon^p, \theta^p, T), \\ p_c(\epsilon^p, \theta^p, T) &= \frac{\partial W^p}{\partial \theta^p}(\epsilon^p, \theta^p, T). \end{aligned} \quad (3.4)$$

Due to material-frame indifference,  $W^e$  can only depend on  $\mathbf{F}^e$  through the corresponding elastic right-Cauchy Green deformation tensor

$$\mathbf{C}^e = \mathbf{F}^{eT} \mathbf{F}^e = \mathbf{F}^{p-T} \mathbf{C} \mathbf{F}^{p-1}. \quad (3.5)$$

Furthermore, the elastic strain-energy density may alternatively be expressed in terms of the logarithmic elastic strain

$$\epsilon^e = \frac{1}{2} \log(\mathbf{C}^e), \quad (3.6)$$

whereupon  $W^e$  takes the form

$$W^e = W^e(\epsilon^e, T). \quad (3.7)$$

We denote by  $\sigma$  the stress conjugate to  $\epsilon^e$ , namely,

$$\sigma = \frac{\partial W^e}{\partial \epsilon^e}(\epsilon^e, T). \quad (3.8)$$

In order to obtain a simple form of  $W^e(\mathbf{C}^e, T)$  we consider a representative neighborhood in the plastically-deformed or ‘intermediate’ configuration of the material. We attribute the volumetric part of  $\mathbf{F}^p$  to void growth, with  $J^p$  related to the current void size through (3.2), and assume that the plastic deformation of the matrix leaves the elastic properties of the matrix unchanged. This assumption is appropriate for metals, whose elastic properties are ostensibly insensitive to isochoric plastic deformation. The plastically deformed configuration can thus be regarded as a two-phase composite consisting of an elastic matrix and a distribution of voids. A simple form of the resulting elastic energy is

$$\begin{aligned} W^e(\epsilon^e, T) &= W^{e,\text{vol}}(\theta^e, T) + W^{e,\text{dev}}(\epsilon^e, T), \\ W^{e,\text{vol}}(\theta^e, T) &= \frac{\kappa}{2} [\theta^e - \alpha(T - T_0)]^2 + \rho_0 C_v T \left(1 - \log \frac{T}{T_0}\right), \\ W^{e,\text{dev}}(\epsilon^e, T) &= \mu \|\text{dev}(\epsilon^e)\|^2, \end{aligned} \quad (3.9)$$

where  $\theta^e = \log J^e$ ,  $\kappa$  is the bulk modulus,  $\mu$  is the shear modulus,  $\alpha$  is the thermal expansion coefficient,  $T_0$  is a reference absolute temperature, and  $C_v$  is the specific heat per unit mass at constant volume.

#### 3.3 Stored energy

A simple stored energy function can be formulated by assuming an additive decomposition into deviatoric and volumetric components. The deviatoric part of the stored energy function can be modeled simply by a conventional power-law of hardening. The volumetric part of the stored energy function is attributed directly to void growth. In the dilute limit, the total energy stored by the void ensemble is the sum of the energy stored by each individual void. The stored energy for a spherical void in a power-law hardening material, which equals the plastic work of deformation attendant to the expansion of the void, has been determined by Molinari and Ortiz [18]. These considerations applied to a spherical shell model lead to the stored energy function

$$\begin{aligned} W^p(\epsilon^p, \theta^p, T) &= W^{p,\text{vol}}(\theta^p, T) + W^{p,\text{dev}}(\epsilon^p, T), \\ W^{p,\text{vol}}(\theta^p, T) &= \frac{n\sigma_0(T)\epsilon_0^p}{n+1} N \frac{4\pi a^3}{3} g(\theta^p, n), \\ W^{p,\text{dev}}(\epsilon^p, T) &= \frac{n\sigma_0(T)\epsilon_0^p}{n+1} \left(1 + \frac{\epsilon^p}{\epsilon_0^p}\right)^{\frac{n+1}{n}}, \end{aligned} \quad (3.10)$$

where

$$g(\theta^p, n) = \int_1^{\frac{1}{J}} \left(1 + \frac{2}{3\epsilon_0^p} \log \frac{x}{x-1 + \frac{f_0}{f_0 + \exp \theta^p - 1}}\right)^{\frac{n+1}{n}} dx. \quad (3.11)$$

In these expressions,  $n$  is the hardening exponent,  $\sigma_0(T)$  is the yield stress, and  $\epsilon_0^p$  is a reference deviatoric plastic strain. The yield stress is assumed to depend on temperature as

$$\sigma_0(T) = \sigma_0(T_0) \left(1 - \frac{T - T_0}{T_m}\right)^l, \quad (3.12)$$

where  $T_0$  is a reference temperature,  $T_m$  is the melting temperature and  $l$  is a thermal-softening exponent.

### 3.4 Rate sensitivity

We consider two types of rate effects: rate sensitivity in the plastic deformation and microinertia due to expanding voids. The deviatoric rate sensitivity may be modeled simply by means of a conventional power-law of hardening. In the dilute limit, the volumetric component of  $\psi^*$  is the sum of all contributions from the individual voids. Based on these considerations, the analysis of Molinari and Ortiz [18], and the same approach as in the previous section, we have

$$\begin{aligned} \psi^*(\dot{\epsilon}^p, \dot{\theta}^p, J^p, T) &= \psi^{*,\text{vol}}(\dot{\theta}^p, J^p, T) + \psi^{*,\text{dev}}(\dot{\epsilon}^p, T), \\ \psi^{*,\text{vol}}(\dot{\theta}^p, J^p, T) &= \frac{m^2 \sigma_0(T) \epsilon_0^p}{m+1} N \frac{4\pi a^3}{3} (1 - f^{\frac{1}{m}}) \left| \frac{2\dot{a}}{\dot{\epsilon}_0^p a} \right|^{\frac{m+1}{m}}, \\ \psi^{*,\text{dev}}(\dot{\epsilon}^p, T) &= \frac{m \sigma_0(T) \epsilon_0^p}{m+1} \left( \frac{\dot{\epsilon}^p}{\dot{\epsilon}_0^p} \right)^{\frac{m+1}{m}}. \end{aligned} \quad (3.13)$$

In these expressions,  $m$  is the rate sensitivity exponent,  $\dot{\epsilon}_0^p$  is a reference plastic strain rate, and  $a$  is regarded as a function of  $J^p$  through (3.2). In addition, by virtue of (3.2), the dependence of  $\psi^*$  on  $|\dot{a}/a|$  induces a dependence on  $|(d/dt) \log J^p|$ , or, in view of (2.7), on  $\dot{\theta}^p$ .

### 3.5 Microinertia

The microinertia attendant to dynamic void growth can be regarded as dissipated energy. In the dilute limit, the total kinetic energy attendant to the growth of the void ensemble is the sum of the kinetic energies due to the expansion of each individual void. For spherical voids in an incompressible material this *microkinetic energy* can be computed readily in terms of the void radius (e.g., [18]), with the result

$$L(a, \dot{a}) = \frac{3}{2} \rho_v(a) \dot{a}^2, \quad \rho_v(a) = \rho_0 N \frac{4\pi a^3}{3}, \quad (3.14)$$

where for simplicity we have neglected a factor of  $(1 - f^{\frac{1}{3}})$ . We note that the kinetic energy  $L$  may instead be written as a function of the variables  $(J^p, \dot{a})$  using relation (3.2).

Note that (3.14) describes a collection of noninteracting particles, each with variable effective mass

$$m(a) = 4\pi \rho_0 a^3. \quad (3.15)$$

In order to facilitate the formulation of variational updates, it proves convenient to effect a change of variables resulting

in a system of particles with constant mass. To this end, we consider now a change of the form  $a = F(b)$ , whereupon (3.14) becomes

$$L(b, \dot{b}) = \frac{3}{2} \rho_v(F(b)) F'^2(b) \dot{b}^2. \quad (3.16)$$

In order to obtain an equivalent system with constant mass, we must choose  $F(b)$  such that

$$\rho_v(F(b)) F'^2(b) = \rho_{v0} \equiv \rho_0 N \frac{4\pi a_0^3}{3}. \quad (3.17)$$

This ordinary differential equation is separable and, therefore, it can be solved explicitly, with the result

$$L(b, \dot{b}) = \frac{3}{2} \rho_{v0} \dot{b}^2, \quad b = \frac{2}{5} \frac{a^{5/2}}{a_0^{3/2}}, \quad (3.18)$$

which corresponds to a system of noninteracting particles with constant mass, as desired.

## 4 Constitutive updates

An incremental solution procedure with time intervals  $[t_n, t_{n+1}]$  is used for the time integration of the constitutive equations. Assume that the state of the material,  $\mathbf{F}_n^p$ ,  $\epsilon_n^p$ ,  $\theta_n^p$ ,  $\dot{\theta}_n^p$  and  $\dot{\theta}_n^p$ , is known at time  $t_n$ , and let the deformation gradient  $\mathbf{F}_{n+1}$  and the temperature  $T_{n+1}$  at time  $t_{n+1}$  be given. The problem is then to determine the state of material,  $\mathbf{F}_{n+1}^p$ ,  $\epsilon_{n+1}^p$ ,  $\theta_{n+1}^p$ ,  $\dot{\theta}_{n+1}^p$  and  $\ddot{\theta}_{n+1}^p$ , at time  $t_{n+1}$ , as well as the directions  $\mathbf{M}$ ,  $\mathbf{N}$  of the incremental plastic deformation, and also the value of the Piola-Kirchhoff stress  $\mathbf{P}_{n+1}$  and the tangent moduli  $D\mathbf{P}_{n+1}$ .

We start by discretizing the flow rule in time using the exponential mapping [7], with the result

$$\mathbf{F}_{n+1}^p = \exp(\Delta \epsilon^p \mathbf{M} + \Delta \theta^p \mathbf{N}) \mathbf{F}_n^p. \quad (4.1)$$

We update the remaining internal state variables,  $\epsilon_{n+1}^p$  and  $\theta_{n+1}^p$ , and simultaneously determine the incremental direction of plastic flow,  $\mathbf{M}$  and  $\mathbf{N}$ , for the time step by recourse to the variational formulation of Ortiz and Stainier [20].

The differential equations of motion for the growth of the voids are second order in time due to microinertia. In order to formulate updates possessing a variational structure, the time-discretization of the equations of motion must itself possess an incremental variational structure. Radovitzky and Ortiz [22] have shown that Newmark's algorithm, when applied to systems with quadratic inertia and constant mass such as (3.14), leads to a minimum problem for the incremental displacements. Thus, we introduce the Newmark predictor

$$b_{n+1}^{\text{pre}} = b_n + \Delta t \dot{b}_n + \left(\frac{1}{2} - \beta\right) \Delta t^2 \ddot{b}_n, \quad (4.2)$$

where  $\beta \in (0, 1/2)$ . We may now introduce the incremental objective function

$$\begin{aligned} f_n(\mathbf{F}_{n+1}^p, \epsilon_{n+1}^p, \theta_{n+1}^p, T_{n+1}, \mathbf{M}, \mathbf{N}) &= \\ W^e(\epsilon_{n+1}^e, T_{n+1}) + W^p(\epsilon_{n+1}^p, \theta_{n+1}^p, T_{n+1}) &+ \\ \Delta t \psi_{n+1}^* + \beta \Delta t^2 B_{n+1}, \end{aligned} \quad (4.3)$$

where  $\Delta t = t_{n+1} - t_n$ , and

$$\begin{aligned}\psi_{n+1}^* &= \psi^* \left( \frac{\Delta \epsilon^p}{\Delta t}, \frac{\Delta \theta^p}{\Delta t}, J_{n+1}^p, T_{n+1} \right), \\ B_{n+1} &= \frac{3\rho_{v0}}{2} \left( \frac{b_{n+1} - b_{n+1}^{\text{pre}}}{\beta \Delta t^2} \right)^2,\end{aligned}\quad (4.4)$$

where  $\Delta \epsilon^p = \epsilon_{n+1}^p - \epsilon_n^p$ ,  $\Delta \theta^p = \theta_{n+1}^p - \theta_n^p$ , and  $b_{n+1}$  is to be regarded as a function of  $J_{n+1}^p$  through (3.18) and (3.2).

Thus the update may be expressed in variational form as

$$W_n(\mathbf{F}_{n+1}, T_{n+1}) = \min_{\epsilon_{n+1}^p, \theta_{n+1}^p, \mathbf{M}, \mathbf{N}} f_n(\mathbf{F}_{n+1}, T_{n+1}, \epsilon_{n+1}^p, \theta_{n+1}^p, \mathbf{M}, \mathbf{N}), \quad (4.5)$$

subject to the constraints (2.5), which define the kinematics of plastic deformation, and the plastic irreversibly constraints

$$\Delta \epsilon^p \geq 0, \quad \Delta \theta^p \geq 0. \quad (4.6)$$

Eq. (4.5) also defines the effective incremental strain-energy density  $W_n(\mathbf{F}_{n+1}, T_{n+1})$  as the minimum of  $f_n$ . Finally, the Newmark correctors

$$\begin{aligned}\dot{b}_{n+1} &= \dot{b}_n + \Delta t[(1 - \gamma)\ddot{b}_n + \gamma\ddot{b}_{n+1}], \\ \ddot{b}_{n+1} &= \frac{b_{n+1} - b_{n+1}^{\text{pre}}}{\beta \Delta t^2},\end{aligned}\quad (4.7)$$

where  $\gamma \in [0, 1]$ , complete the update.

The effective work of deformation density (4.5) returns the updated values of the internal variables and the direction of plastic flow over the time step. Moreover,  $W_n(\mathbf{F}_{n+1})$  acts as a potential for the first Piola-Kirchhoff stress tensor  $\mathbf{P}_{n+1}$  at time  $t_{n+1}$ . In order to prove this property, suppose that the deformation gradient  $\mathbf{F}_{n+1}$  is perturbed to  $\mathbf{F}_{n+1} + \delta \mathbf{F}_{n+1}$ . The corresponding variation of the effective work of deformation density (4.5) reads

$$\begin{aligned}\delta W_n &= \frac{\partial W_n^e}{\partial \mathbf{F}_{n+1}} \cdot \delta \mathbf{F}_{n+1} + \\ &\frac{\partial W_n}{\partial \epsilon_{n+1}^p} \delta \epsilon_{n+1}^p + \frac{\partial W_n}{\partial \theta_{n+1}^p} \delta \theta_{n+1}^p + \frac{\partial W_n}{\partial \mathbf{M}} \cdot \delta \mathbf{M} + \frac{\partial W_n}{\partial \mathbf{N}} \cdot \delta \mathbf{N}.\end{aligned}\quad (4.8)$$

The last four terms in this identity vanish due to stationarity. In addition, we have

$$\mathbf{P}_{n+1} = \frac{\partial W_n^e}{\partial \mathbf{F}_{n+1}}, \quad (4.9)$$

and (4.8) reduces to

$$\delta W_n = \mathbf{P}_{n+1} \cdot \delta \mathbf{F}_{n+1}. \quad (4.10)$$

Since  $\delta \mathbf{F}_{n+1}$  is arbitrary this implies

$$\mathbf{P}_{n+1} = \frac{\partial W_n}{\partial \mathbf{F}_{n+1}}. \quad (4.11)$$

Consequently  $W_n$  acts as a potential for first Piola-Kirchhoff stresses  $\mathbf{P}_{n+1}$  and the constitutive update possesses an incremental potential structure. The tangent moduli corresponding

to the variational updates follow by linearization of (4.11). This gives

$$D\mathbf{P}_{n+1} = \frac{\partial^2 W_n}{\partial \mathbf{F}_{n+1} \partial \mathbf{F}_{n+1}}. \quad (4.12)$$

The tangent moduli are symmetric owing to the potential character of the incremental stress-strain relation.

## 5 Implementation based on logarithmic elastic strains

As noted by Cuitiño and Ortiz [7], and by Ortiz and Stainier [20], formulations based on logarithmic elastic strains effectively reduce finite-deformation updates to small-strain updates and pre- and post-processing steps which are purely kinematic and, therefore, material-independent. Let

$$\mathbf{C}_{n+1}^{e, \text{pre}} = \mathbf{F}_n^{p-T} \mathbf{C}_{n+1} \mathbf{F}_n^{p-1} \quad (5.1)$$

be the trial or predictor elastic right Cauchy-Green deformation tensor obtained by assuming no incremental plastic deformation, and suppose that the commutation relation

$$\mathbf{M} \mathbf{C}_{n+1}^{e, \text{pre}} = \mathbf{C}_{n+1}^{e, \text{pre}} \mathbf{M} \quad (5.2)$$

holds between  $\mathbf{C}_{n+1}^{e, \text{pre}}$  and the direction of plastic flow  $\mathbf{M}$  for the same step, which means that both tensors have the same set of eigenvectors. Then, by the properties of the exponential, we have

$$\epsilon_{n+1}^e = \epsilon_{n+1}^{e, \text{pre}} - \Delta \epsilon^p \mathbf{M} - \Delta \theta^p \mathbf{N}, \quad (5.3)$$

where

$$\epsilon_{n+1}^{e, \text{pre}} = \frac{1}{2} \log(\mathbf{C}_{n+1}^{e, \text{pre}}) \quad (5.4)$$

is the trial or predictor value of the logarithmic elastic strain. Using these identities, the objective function (4.3) obtains an additive structure in terms of elastic and plastic deformations which is entirely analogous to that of small-strain plasticity. In particular, in simple cases, such as that of an elastic strain-energy density  $W^e$  quadratic in  $\epsilon^e$ , the minimization of  $f_n$  with respect to  $\epsilon_{n+1}^p$ ,  $\theta_{n+1}^p$ ,  $\mathbf{M}$  and  $\mathbf{N}$  can be carried out explicitly.

The stress-strain relations follow by an application of the chain rule, with the result

$$\mathbf{P}_{n+1} = \frac{\partial W_n}{\partial \mathbf{F}_{n+1}} = \frac{\partial W_n}{\partial \epsilon_{n+1}^e} \cdot \frac{\partial \epsilon_{n+1}^e}{\partial \mathbf{C}_{n+1}} \cdot \frac{\partial \mathbf{C}_{n+1}}{\partial \mathbf{F}_{n+1}}, \quad (5.5)$$

or, in components

$$P_{iJ} = \sigma_{ABD} \log(\mathbf{C}_{n+1}^{e, \text{pre}})_{ABCD} (\mathbf{F}_n^{p-1})_{JC} (\mathbf{F}_n^{p-1})_{KD} F_{iK}, \quad (5.6)$$

where we have dropped the label  $n+1$  throughout for ease of reading. Differentiating this expression once more gives the consistent tangents in the form

$$\begin{aligned}DP_{iJkL} &= \\ &\delta_{ik} \sigma_{ABD} D \log(\mathbf{C}_{n+1}^{e, \text{pre}})_{ABCD} (\mathbf{F}_n^{p-1})_{JC} (\mathbf{F}_n^{p-1})_{LD} + \\ &[D \sigma_{ABCD} D \log(\mathbf{C}_{n+1}^{e, \text{pre}})_{ABEF} (\mathbf{F}_n^{p-1})_{JE} (\mathbf{F}_n^{p-1})_{KF} \\ &D \log(\mathbf{C}_{n+1}^{e, \text{pre}})_{CDGH} (\mathbf{F}_n^{p-1})_{LG} (\mathbf{F}_n^{p-1})_{MH} + \\ &2\sigma_{ABD} D^2 \log(\mathbf{C}_{n+1}^{e, \text{pre}})_{ABEFGH} \\ &(\mathbf{F}_n^{p-1})_{JE} (\mathbf{F}_n^{p-1})_{KF} (\mathbf{F}_n^{p-1})_{LG} (\mathbf{F}_n^{p-1})_{MH}] F_{iK} F_{kM}.\end{aligned}\quad (5.7)$$

Explicit expressions for the efficient calculation of the first and second linearizations of the logarithmic mapping have been given by Ortiz et al. [19].

Minimization of  $f_n$  with respect to  $M$  and  $N$ , subject to the constraints (2.5) gives, after some algebraic manipulation,

$$M = \frac{3s_{n+1}^{\text{pre}}}{2\sigma_{n+1}^{\text{pre}}}, \quad N = \frac{1}{3}\text{sgn}(p_{n+1}^{\text{pre}})\mathbf{I}, \quad (5.8)$$

where

$$\begin{aligned} s_{n+1}^{\text{pre}} &= 2\mu\text{dev}(\epsilon_{n+1}^{e,\text{pre}}), \\ \sigma_{n+1}^{\text{pre}} &= \sqrt{(3/2)s_{n+1}^{\text{pre}} \cdot s_{n+1}^{\text{pre}}}, \\ p_{n+1}^{\text{pre}} &= \kappa [\text{tr}(\epsilon_{n+1}^{e,\text{pre}}) - \alpha(T_{n+1} - T_0)], \end{aligned} \quad (5.9)$$

can be computed explicitly from the initial data for the time step. Thus, the effective Mises stress and the magnitude of the pressure are found to be the thermodynamic forces driving  $\epsilon^p$  and  $\theta^p$ , respectively.

Minimization with respect to  $\epsilon_{n+1}^p$  and  $\theta_{n+1}^p$  gives

$$\begin{aligned} \Delta\epsilon^p &= \epsilon_{n+1}^p - \epsilon_n^p = 0, \\ \Delta\theta^p &= \theta_{n+1}^p - \theta_n^p = 0, \end{aligned} \quad (5.10)$$

if

$$\begin{aligned} \sigma_{n+1}^{\text{pre}} &\leq \sigma_c(\epsilon_n^p, \theta_n^p, T_{n+1}), \\ p_{n+1}^{\text{pre}} &\leq p_c(\epsilon_n^p, \theta_n^p, T_{n+1}), \end{aligned} \quad (5.11)$$

or

$$\begin{aligned} \sigma_{n+1}^{\text{pre}} - 3\mu\Delta\epsilon^p &= \sigma_{c,n+1} + \frac{\partial}{\partial\epsilon_{n+1}^p} [\Delta t \psi_{n+1}^* + \beta\Delta t^2 B_{n+1}], \\ p_{n+1}^{\text{pre}} - \kappa\Delta\theta^p &= p_{c,n+1} + \frac{\partial}{\partial\theta_{n+1}^p} [\Delta t \psi_{n+1}^* + \beta\Delta t^2 B_{n+1}], \end{aligned} \quad (5.12)$$

otherwise.

## 6 Examples of predicted material behavior

An area of application where microinertia is potentially important is the propagation of shocks in metals. The deformations of interest in this case are of uniaxial strain, and the corresponding deformation gradients are of the form  $\mathbf{F} = \text{diag}\{\lambda, 1, 1\}$ , for some uniaxial stretch ratio  $\lambda$ . This type of deformation combines volumetric and deviatoric deformations, and thus illustrates many of the features of the model presented in the foregoing. Unless otherwise indicated, the material parameters used in all examples are as in Table 1.

For the simple case of uniaxial strain, the elastic deformation is of the form  $\mathbf{F}^e = \text{diag}\{\lambda^e, \lambda_T^e, \lambda_T^e\}$ , where  $\lambda^e$  and  $\lambda_T^e$  are the longitudinal and transverse stretch ratios, respectively, and the plastic deformation is of the form  $\mathbf{F}^p = \text{diag}\{\lambda^p, \lambda_T^p, \lambda_T^p\}$ , where  $\lambda^p$  and  $\lambda_T^p$  are the longitudinal and transverse stretch ratios, respectively.

$E$ [GPa]	$\nu$	$\sigma_0(T_0)$ [MPa]	$\epsilon_0^p$	$n$	$a_0$ [ $\mu\text{m}$ ]	$\rho_0$ [ $\text{kg m}^{-3}$ ]
165	0.15	600	0.01	10	100	17300
$N$ [ $\text{m}^{-3}$ ]	$\epsilon_0^p$	$m$	$T_0$ [K]	$T_m$ [K]	$l$	$\alpha$ [ $\text{K}^{-1}$ ]
$10^{10}$	0.001	10	293	1400	0.75	$42 \times 10^{-6}$

**Table 1** Material parameters used in the examples of Section 6

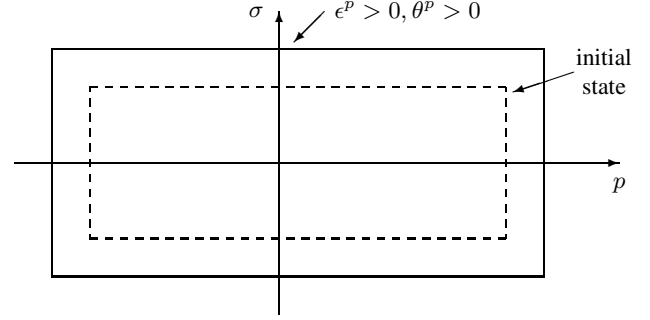


**Fig. 6.1** Yield locus in the pressure-Mises stress plane.

### 6.1 Yield phenomena

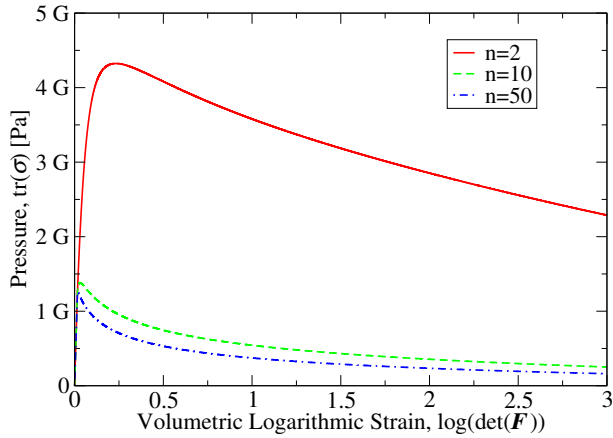
The elastic domain at initial state  $\mathbf{F}^p = \mathbf{I}$ ,  $\epsilon^p = 0$ ,  $\theta^p = 0$  and a second state  $\mathbf{F}^p \neq \mathbf{I}$ ,  $\epsilon^p > 0$ ,  $\theta^p > 0$  are shown in Fig. 6.1 on the  $(p, \sigma)$ -plane. The deviatoric and volumetric parts of the yield surface intersect discontinuously, resulting in a corner. This is in contrast to models such as Gurson's and extensions thereof [10; 28], in which the yield surface is smooth.

During deformation the voids may further expand or collapse under the action of positive and negative pressures, respectively. Note that the processes of void expansion and collapse are predicted to be asymmetric, with the magnitude of the critical pressure for void collapse being smaller than the critical pressure for void expansion. Once the voids are collapsed the plastic response of the material becomes insensitive to negative pressure.

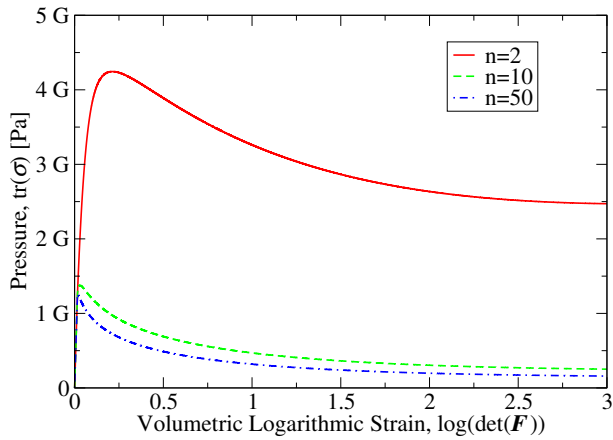
### 6.2 Hardening

The volumetric response predicted by the model is of primary interest in applications. In order to exhibit this response, we begin by applying a monotonically increasing, quasistatic, pure volumetric deformation to the material. Fig. 6.2a shows the dependence of the matrix pressure  $\text{tr}\sigma$  on the logarithmic volumetric strain  $\theta^p$  for three values of the hardening exponent  $n$ . As may be seen from this plot, the behavior of the material is ostensibly linear elastic prior to the attainment of the critical pressure. At this point the material yields and starts deforming plastically involving strain softening, i.e.,  $p \rightarrow 0$  as  $\theta^p \rightarrow \infty$ .

The behavior at large volumetric strains in a uniaxial strain state is displayed in Fig. 6.2b in terms of the volumetric component of the stress tensor  $\text{tr}\sigma$ . Here the interaction of volumetric strain softening and deviatoric strain hardening leads



(a)



(b)

**Fig. 6.2** Quasistatic monotonic response for three different hardening exponents. a) Matrix pressure in hydrostatic loading. b) Volumetric component of the stress tensor in uniaxial strain.

to an approximately constant value of the pressure as the strain increases.

### 6.3 Microinertia

At high rates of deformation void growth may significantly be retarded by microinertia [18; 16; 13; 17]. Microinertia may be expected to be significant when  $\dot{\theta}$  becomes comparable to  $c/a$ , where  $c$  is the elastic sound speed. In order to exhibit this behavior, we artificially turn off rate sensitivity, and subject the material to a constant rate of volumetric expansion. The resulting volumetric stress-strain curve is shown in Fig. 6.3. As may be seen from the figure, the volumetric stress-strain behavior is ostensibly indistinguishable from the quasistatic behavior for small rates of deformation. For rates comparable to the threshold  $c/a = 3.7 \times 10^7 \text{s}^{-1}$ , the stress-

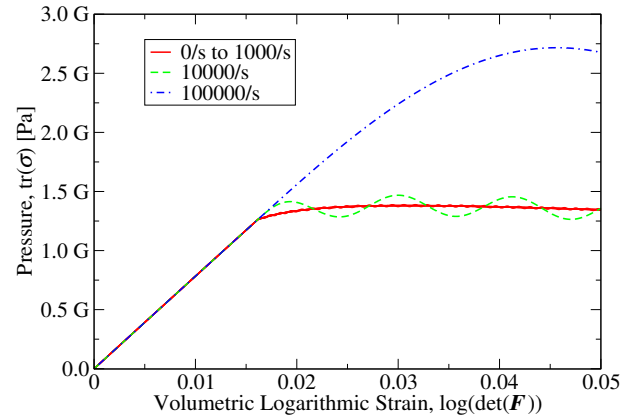


**Fig. 6.3** Effect of microinertia on the volumetric stress-strain relation.

strain curve depends sensitively on the rate of deformation and effects a smooth transition from strain softening to initially elastic curves as the strain rate increases. As the expansion continues, the pressure exhibits oscillations with amplitude and wave length proportional to the volumetric strain rate. This behavior is expected as the differential equations of motion for the growth of the voids in the model are of second order in time.

## 7 Application example

An example of the versatility of the porous plasticity model developed here is the simulation of the forced expansion and ductile fracture and fragmentation of U-6%Nb rings. An outward radial force is applied to the rings by a driver ring, which in turn interacts with a solenoid. When current is applied to the solenoid, a magnetic force is induced in the driver ring creating a uniform radial body force. The U-6%Nb rings are thus forced to expand and eventually fracture dynamically [4]. The U-6%Nb rings have an inner diameter of 34.37mm, an outer diameter of 35.89mm, and thickness of 0.76mm. An arrestor ledge in the experimental device prevents the driver ring to expand beyond a diameter of 40.0mm, but the U-6%Nb rings are allowed to expand driven by their kinetic energy, until they eventually fracture and fragment. The initial velocity history applied to the U-6%Nb rings varies according to three different accelerating voltages of 5.0kV, 6.0kV, and 7.5kV [4].

The U-6%Nb alloy is modeled by using the porous plasticity model developed here in conjunction with the strain localization model developed by Yang et al. [29], which is specially well-suited for the simulation of nucleation and propagation of ductile fracture. The ring is subjected to high velocity loading, therefore the analysis is performed using explicit dynamics and assuming adiabatic heating. The finite element mesh used in our simulations is shown in Figure 7.1. The initial number of nodes is 2634 and the initial number of tetrahedral elements is 882. The nucleation and propagation of fracture is simulated by adaptively inserting surface-like strain lo-

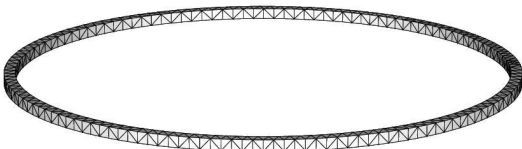
calization elements between bulk elements when  $\epsilon^p \geq 0.4$  at the interface. This value is representative of the critical plastic strain for metal ring fragmentation at high strain rates observed in experiments [9]. The material parameters used in the calculation are as shown in Table 2.

$E$ [GPa]	$\nu$	$\sigma_0(T_0)$ [MPa]	$\epsilon_0^p$	$n$	$a_0$ [ $\mu\text{m}$ ]	$\rho_0$ [ $\text{kg m}^{-3}$ ]
165	0.15	600	0.01	10	100	17300
$N$ [ $\text{m}^{-3}$ ]	$\epsilon_0^p$	$m$	$T_0$ [K]	$T_m$ [K]	$l$	$\alpha$ [ $\text{K}^{-1}$ ]
$10^{10}$	0.001	500	293	1400	0.75	$42 \times 10^{-6}$

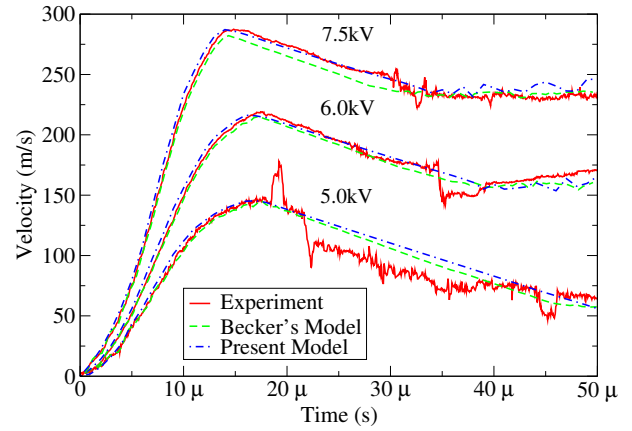
**Table 2** Material parameters for U-6%Nb alloy.

Figure 7.2 shows the calculated and experimental velocity histories reported by Becker [4], as well as the velocity histories obtained in our simulations. The radial velocity of all the nodes on the inner radius is initially prescribed to match the radial velocity of the driver ring, as measured by experiments [4], up to the peak velocity for each curve in Figure 7.2. The figure shows that after release there is a noticeable decrease in velocity which can be attributed to kinetic energy being converted to plastic deformation. The region in which the curves become irregular and constant on average is where fracture has occurred. We see from Figure 7.2 that our calculations capture very well the region of plastic flow and the initiation of fracture and fragmentation as measured by experiments. It is also remarkable the closeness of our calculations to those of Becker [4], considering that the mesh used in our calculation is much coarser (882 vs. 15000 elements).

A sequence of frames of the fracture and fragmentation of the U-6%Nb rings for the case of an applied voltage of 7.5kV is shown in Figure 7.3. The elapsed time between frames is  $30\mu\text{s}$ , and the color bar indicates the value of the plastic strain. For this particular voltage, the time when fracture starts to occur is approximately  $30\mu\text{s}$  [4]. The figure clearly shows the expansion of the ring and the process of fracture and fragmentation that begins around  $30\mu\text{s}$ . The number of major fragments obtained in the simulation is 26, compared to 19 fragments as observed in experiments [4]. In both cases the number of fragments was determined visually.



**Fig. 7.1** Finite element mesh for U-6%Nb rings: 2634 nodes, 882 elements.



**Fig. 7.2** Velocity history for U-6%Nb rings. Experimental data taken from Becker [4].

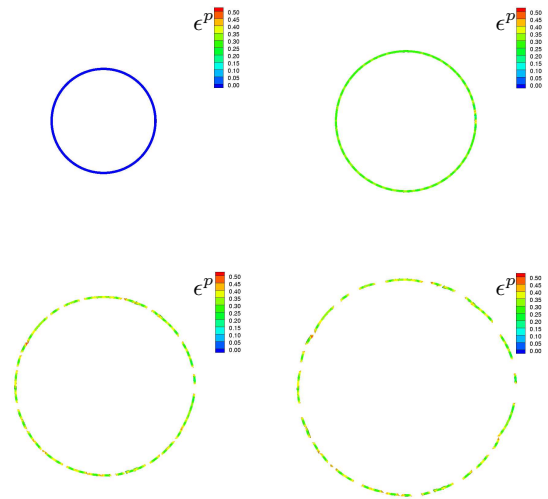


**Fig. 7.3** Dynamic fracture and fragmentation of U-6%Nb rings. Configurations at  $0\mu\text{s}$ ,  $30\mu\text{s}$ ,  $60\mu\text{s}$  and  $90\mu\text{s}$ .

## 8 Concluding remarks

We have developed a variational finite-deformation framework for the modeling of ductile damage by void growth in metals. The specific model presented in this paper exploits the void growth ideas of Ortiz and Molinari [18]. The constitutive relations are discretized in time by means of the variational update of Ortiz and Stainier [20]. The resulting *engineering* model and constitutive updates provide a fully variational alternative to Gurson-like models. In particular, the present variational update decouples finite volumetric and deviatoric deformations, is exactly material-frame indifferent under finite rotations, and results in symmetric tangent moduli.

The framework presented in this paper puts forth a workable set of constitutive functions to be modeled or identified, namely, the elastic energy density, the stored energy function, the dual rate-sensitivity potential and the microinertia density. For actual materials, this identification can be achieved, e.g., by analyzing a periodic distribution of voids in a single crystal.

The predictive capabilities of the model are demonstrated by the finite element simulation of the forced expansion and fragmentation of U-6%Nb rings. Comparisons of the velocity histories and number of fragments show that the results of the calculations are in very good agreement with experimental observations.

## 9 Acknowledgments

We are grateful for the financial support provided by the US Department of Energy through Caltechs ASC Center for the Simulation of the Dynamic Response of Materials.

## References

1. J.M. Ball. Discontinuous equilibrium solutions and cavitation in non-linear elasticity. *Philos. T. Roy. Soc. A*, 306(1496):557–611, 1982.
2. T.W. Barbee, L. Seaman, R. Crewdson, and D. Curran. Dynamic fracture criteria for ductile and brittle metals. *J. Mater.*, 7(3):393–401, 1972.
3. C.D. Beachem and G.R. Yoder. Elastic-plastic fracture by homogeneous microvoid coalescence tearing along alternating shear planes. *Metall. Trans.*, 4(4):1145–1153, 1973.
4. R. Becker. Ring fragmentation predictions using the gurson model with material stability conditions as failure criteria. *Int. J. Solids Struct.*, 39(13-14):3555–3580, 2002.
5. J. Belak. On the nucleation and growth of voids at high strain-rates. *J. Comput.-Aided Mater.*, 5:193–206, 1998.
6. R. Cortes. Dynamic growth of microvoids under combined hydrostatic and deviatoric stresses. *Int. J. Solids Struct.*, 29(13):1637–1645, 1992.
7. A. Cuitino and M. Ortiz. A material-independent method for extending stress update algorithms from small-strain plasticity to finite plasticity with multiplicative kinematics. *Eng. Computation*, 9:255–263, 1992.
8. B.L. Glushak, S.V. Koritskaya, and I.R. Trunin. Numerical analysis of damage accumulation in copper under dynamic load. *Chem. Phys. Rep.*, 18(10-11):1835–1841, 2000.
9. D.E. Grady and D.A. Benson. Fragmentation of metal rings by electromagnetic loading. *Exp. Mech.*, 23(4):393–400, 1983.
10. A.L. Gurson. Continuum theory of ductile rupture by void nucleation and growth: Part 1: Yield criteria and flow rules for porous ductile media. *J. Eng. Mater.-T. ASME*, 99(1):2–15, 1977.
11. K. Hackl. Generalized standard media and variational principles in classical and finite strain elastoplasticity. *J. Mech. Phys. Solids*, 45(5):667–688, 1997.
12. Y. Huang, J.W. Hutchinson, and V. Tvergaard. Cavitation instabilities in elastic plastic solids. *J. Mech. Phys. Solids*, 39(2):223–241, 1991.
13. J.B. Leblond and G. Roy. A model for dynamic ductile behavior applicable for arbitrary triaxialities. *CR Acad. Sci. II B*, 328(5):381–386, 2000.
14. E.H. Lee. Elastic-plastic deformation at finite strains. *J. Appl. Mech.*, 36(1):1–6, 1969.
15. J. Lubliner. On the thermodynamic foundations of non-linear solid mechanics. *Int. J. Nonlinear Mech.*, 7:237–254, 1972.
16. S. Mercier and A. Molinari. Micromechanics of void growth at high rates. *J. Phys. IV*, 10(P9):415–420, 2000.
17. A. Molinari and S. Mercier. Micromechanical modelling of porous materials under dynamic loading. *J. Mech. Phys. Solids*, 49(7):1497–1516, 2001.
18. M. Ortiz and A. Molinari. Effect of strain-hardening and rate sensitivity on the dynamic growth of a void in a plastic material. *J. Appl. Mech.-T. ASME*, 59(1):48–53, 1992.
19. M. Ortiz, R.A. Radovitzky, and E.A. Repetto. The computation of the exponential and logarithmic mappings and their first and second linearizations. *Int. J. Numer. Meth. Eng.*, 52(12):1431–1441, 2001.
20. M. Ortiz and L. Stainier. The variational formulation of viscoplastic constitutive updates. *Comput. Method. Appl. M.*, 171(3-4):419–444, 1999.
21. P. Perzyna. Internal state variable description of dynamic fracture of ductile solids. *Int. J. Solids Struct.*, 22(7):797–818, 1986.
22. R. Radovitzky and M. Ortiz. Error estimation and adaptive meshing in strongly nonlinear dynamic problems. *Comput. Method. Appl. M.*, 172(1-4):203–240, 1999.
23. P.F. Thomason. *Ductile fracture of metals*. Pergamon Press, New York, 1990.
24. P.F. Thomason. Ductile spallation fracture and the mechanics of void growth and coalescence under shock-loading conditions. *Acta Mater.*, 47(13):3633–3646, 1999.
25. W. Tong and G. Ravichandran. Inertial effects on void growth in porous viscoplastic materials. *J. Appl. Mech.-T. ASME*, 62(3):633–639, 1995.
26. V. Tvergaard. Material failure by void growth to coalescence. *Adv. Appl. Mech.*, 27:83–151, 1990.
27. V. Tvergaard, Y. Huang, and J.W. Hutchinson. Cavitation instabilities in a power hardening elastic-plastic solid. *Eur. J. Mech. A-Solid.*, 11(2):215–231, 1992.
28. V. Tvergaard and A. Needleman. Analysis of the cup-cone fracture in a round tensile bar. *Acta Metall.*, 32(1):157–169, 1984.
29. Q. Yang, A. Mota, and M. Ortiz. A class of variational strain-localization finite elements. *Int. J. Numer. Meth. Eng.*, 2004. submitted.
30. A.K. Zurek, W.R. Thissell, D.L. Tonks, R. Hixson, and F. Addessio. Quantification of damage evolution for a micromechanical model of ductile fracture in spallation of tantalum. *J. Phys. IV*, 7(C3):903–908, 1997.